Water Science & Technology

IWA PUBLISHING

Water Science & Technology Vol 86 No 1, 80 doi: 10.2166/wst.2022.189

Adsorption and removal of direct red 31 by Cu-MOF: optimization by response surface

Zihang Li[a,b], Dajun Ren[a,b,*], Zhaobo Wang[a,b], Shan Jiang[a,b], Shuqin Zhang[a,b], Xiaoqing Zhang[a,b] and Wangsheng Chen[a,b]

[a] College of Resource and Environmental Engineering, Wuhan University of Science and Technology, Wuhan 430081, China
[b] Hubei Key Laboratory for Efficient Utilization and Agglomeration of metallurgic Mineral Resources, Wuhan University of Science and Technology, Wuhan, Hubei 430081, China
*Corresponding author. E-mail: dj_ren@163.com

DR, 0000-0003-0752-4184

ABSTRACT

Cu(PABA) is a Cu-based MOF material assembled from Cu^{2+} and the organic ligand p-aminobenzoic acid (PABA). Cu (PABA) was synthesized by a solvothermal method, characterized and applied to the adsorption of direct red 31 dye (DR-31). The effects of pH, DR-31 concentration and temperature on the adsorption performance of Cu(PABA) were investigated. The adsorption kinetics were analyzed by pseudo-first-order, pseudo-second-order and intra-particle diffusion models, and the adsorption equilibrium data was fitted by Langmuir and Freundlich isotherm models. The pseudo-first-order kinetics and Langmuir model satisfactorily described the adsorption kinetics and adsorption equilibrium, respectively. The maximum adsorption capacity of Cu(PABA) for DR-31 dye at room temperature was 1,244.8 mg/g, as calculated using the Langmuir adsorption isotherm model. By response surface methodology (RSM), the optimal adsorption was found at pH value of 10.9, DR-31 dye concentration of 216.6 mg/L, and temperature of 27 °C, and the removal rate was as high as 99.4%. Therefore, Cu(PABA) can be used as an efficient adsorbent for removing DR-31 dye from aqueous solution.

Key words: adsorption removal, Cu(PABA), DR-31dye, response surface optimization

HIGHLIGHTS

- MOF material Cu(PABA) was synthesized by a solvothermal method.
- The kinetics and isotherm models of DR-31dye adsorption on Cu(PABA) were studied.
- According to the Langmuir isotherm model, the maximum adsorption capacity was calculated to be 1,244.8 mg/g.
- Optimization of DR-31dye adsorption on Cu(PABA) by RSM.

GRAPHICAL ABSTRACT

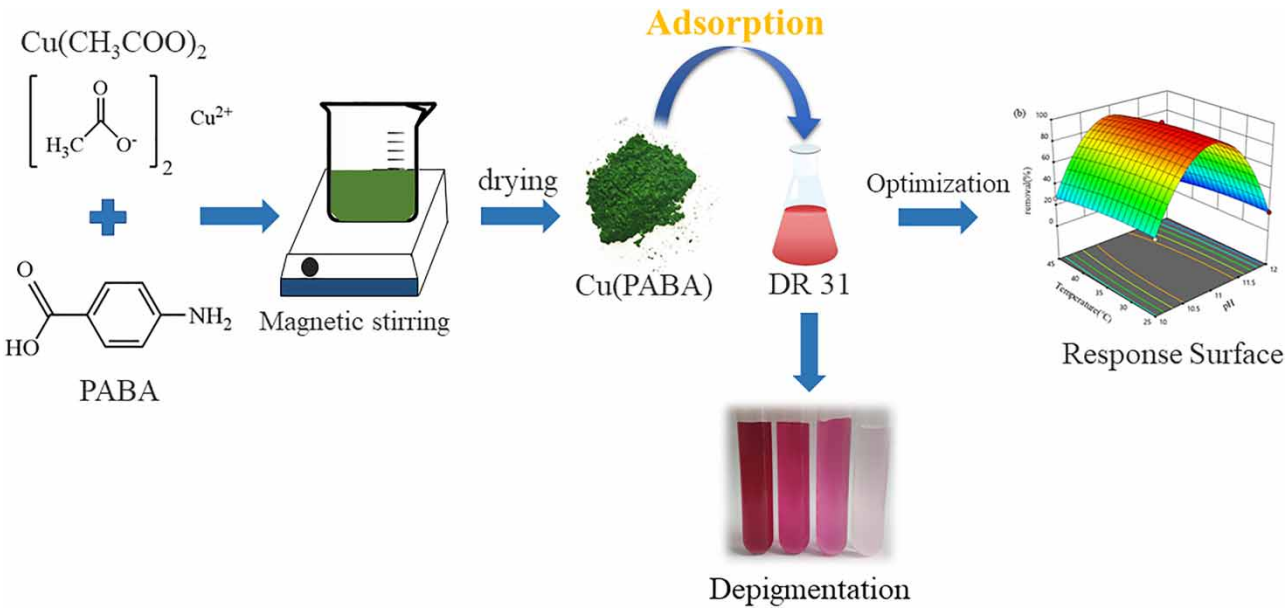

1. INTRODUCTION

Since modern times, dyes have been widely used in various places, such as papermaking, textiles, plastics, food and other industries (Faisal *et al.* 2022). This has resulted in the production of a large amount of wastewater contaminated with dyes. Because dyes are easily diffused, difficult to degrade, and toxic, they are a serious threat to the water environment. Large amounts of dyes are released into the water and accumulate over time, resulting in a decline in water quality and a large number of aquatic life deaths. In addition, some dyes can also endanger human health, cause various diseases, and even cause cancer. Therefore, people have to pay attention to the method of remediation of dye-contaminated water. Direct red 31 (DR-31) dye is a common synthetic dye and is easily soluble in water. It is mostly used for dyeing and printing silk, wool, paper, leather and other fibers, as well as for coloring paint, plastic, rubber, etc (Bhatia *et al.* 2016). DR-31 is an azo dye, which can secrete carcinogens and induce cancer under certain conditions. Therefore, it is necessary to remove it from the water environment.

Dye pollution in wastewater can be removed by physical, chemical or biological methods. Depending on the type of dye, the remediation technologies that can be used for dye wastewater treatment include adsorption, filtration, coagulation, photooxidation, chemical oxidation, ozonation and biodegradation, etc (Katheresan *et al.* 2018). Among these technologies, adsorption technology is one of the most commonly used sewage treatment methods due to its advantages of low cost, high efficiency, more environmental protection, convenient operation and easy recovery and reuse of adsorbents (Chowdhury *et al.* 2020). For adsorption, the removal effect of pollution mainly depends on the adsorption capacity of the adsorbent, so the selection of adsorbent is very important. At present, common adsorbents include zeolite, fly ash, silica gel, activated carbon and chitosan (Sadiq *et al.* 2021). Although these adsorbents are already available, sometimes they cannot achieve satisfactory results, so people hope to develop cheaper and more efficient adsorbents.

Metal organic frameworks (MOFs) are a class of porous hybrid materials, which are formed by the combination of metal ions and organic ligands through coordination bonds. MOFs are widely used in various fields such as gas storage and separation, chemical sensors, electrochemistry, catalysis, adsorption and so on. In the field of adsorption, MOFs are considered to be an ideal adsorption material due to their large surface area, high porosity and adjustable pore size (Oladoye *et al.* 2021). In fact, MOF materials used as adsorbents for heavy metals and organics in water have indeed received a lot of attention in recent decades (Oladoye *et al.* 2021). Cu(PABA) is a kind of Cu-MOF material. There are few reports about it at present, and the use of its pure carrier as an adsorbent to remove the DR-31 dye in water has not been reported.

The adsorption and removal of pollutants by adsorbents is affected by many factors, such as initial concentration, adsorbent dosage, solution pH and temperature. To more reasonably and simply analyze the simultaneous effects of these variables on

adsorption and obtain the ideal restoration effect, we optimized the experimental parameters by using the response surface methodology (RSM). In terms of optimization research, RSM is a proven and useful method. Compared with the commonly used single variable analysis method, RSM comprehensively considers the influence of various parameters, and can significantly reduce the amount of experiments, with obvious advantages.

In this paper, we synthesized the Cu-MOF material Cu(PABA) and used it as an adsorbent to remove DR-31 dye from solution. We investigated adsorption kinetics and adsorption isotherms, and evaluated the remediation ability of Cu(PABA) for DR-31 dye. We used single-factor and multi-factor methods to analyze the effects of the initial concentration of DR-31 dye, pH, and temperature on the adsorption. The experimental parameters were optimized by RSM. The results show that Cu(PABA) has high adsorption capacity and removal rate for DR-31 dye.

2. EXPERIMENTAL

2.1. Materials

All reagents and drugs in this study are of analytical grade and can be used without further purification. Copper acetate monohydrate ($Cu(CH_3COO)_2{\cdot}H_2O$) and p-aminobenzoic acid (PABA) were purchased from Macklin. DR-31 dye was purchased from Shandong Yousu Chemical Technology Co., Ltd. Hydrochloric acid (HCl), sodium hydroxide (NaOH) and methanol (CH_3OH) were all from Sinopharm Chemical Reagent Co., Ltd

2.2. Synthesis of Cu(PABA)

Cu(PABA) was synthesized by a solvothermal method, mixing copper acetate monohydrate ($Cu(CH_3COO)_2{\cdot}H_2O$) and p-aminobenzoic acid(PABA) at a ratio of 1.25:1. In detail, an electronic balance was first used to accurately weigh 0.218 g of $Cu(CH_3COO)_2{\cdot}H_2O$ and 0.120 g of PABA. $Cu(CH_3COO)_2{\cdot}H_2O$ was dissolved in 10 mL pure water, and PABA was dissolved in 6 mL pure water and 4 mL methanol mixed solution. Then, the cup containing $Cu(CH_3COO)_2{\cdot}H_2O$ solution was placed on a magnetic stirrer and PABA solution was added drop by drop. After 6 hours of magnetic stirring, the mixture was centrifuged at 4,000 r. Finally, Cu(PABA) solid can be prepared by drying at 353 K.

2.3. Characterization

Microstructure and morphology of Cu(PABA) were characterized by scanning electron microscope (SEM, Zeiss Sigma300). The functional groups of Cu(PABA) were determined by Thermo Scientific Nicolet 6700 spectrometer, and the spectra were obtained in the scanning range of 400–4,000 cm^{-1}. Thermogravimetric analysis (TGA) was measured using TGA 5500 thermo gravimetric analyzer. The powder samples were heated from 30 °C to 800 °C at a heating rate of 10 °C/min in N_2 atmosphere. The specific surface area and pore size distribution were measured in N_2 atmosphere using the Mike 2460 automatic specific surface and porosity analyzer, where the degassing time was 8 h and the degassing temperature was 200 °C. Surface properties were analyzed using the Thermo Scientific K-Alpha X-ray photoelectron spectrometer.

2.4. Adsorption experiments

Batch adsorption experiments were performed in a thermostatic shaker at 200 rpm with the temperature set to 25 °C. Before adding the adsorbent, a set of 100 mg/L DR-31 dye solutions (pH 3–12) by 0.1 M HCl and NaOH solutions were prepared to explore the effect of pH on adsorption. When studying the effect of initial concentration on adsorption, the concentration range of DR-31 was 50, 100, 150, 200, 250, 300 (mg/L), adding 10 mg Cu(PABA) sample to 50 ml solution. The removal rate(η) and adsorption capacity (q_e) were calculated by formulas (1) and (2), respectively.

$$\eta(\%) = \frac{C_0 - C_e}{C_0} \times 100\% \tag{1}$$

$$q_e = \frac{(C_0 - C_e)V}{m} \tag{2}$$

where C_0 (mg/L) and C_e(mg/L) represent the initial concentration and equilibrium concentration of DR-31 solution, respectively; V(L) is the volume of the solution; m(g) Represents the quality of input Cu(PABA).

Kinetics were performed using an initial DR-31 concentration of 150 mg/L at a pH of 11. The isotherms were performed at three temperatures (25 °C, 35 °C, 45 °C) to observe the effect of temperature on adsorption. All absorbances were measured

using a UV-2550 UV-Vis spectrometer. The maximum absorption wavelength of DR-31 is 525 nm, and the concentration of DR-31 was calculated by the change of absorbance at this wavelength.

2.5. RSM optimization

In this study, the combined interference of various parameters (pH, DR-31 dye concentration and temperature) on adsorption was evaluated using the RSM approach. BOX-Behnken design (BBD) was used to determine the optimum process parameters. The design model of three levels and three factors was adopted. Three codes of −1, 0 and +1 represented three levels (high, medium and low). A, B and C corresponded to three factors of pH, DR-31 dye concentration and temperature, respectively. Table 1 shows the experimental design levels for the DR-31 dye adsorption factor on Cu(PABA).

Based on the interaction between parameters, the mathematical expression of adsorption can be listed

$$Y = \beta_0 + \Sigma_{i=1}^{K}\beta_i X_i + \Sigma_{i=1}^{K}\beta_{ii}X_i^2 + \Sigma_i^{K-1}\Sigma_j^{K}\beta_{ij}X_iX_j \quad (3)$$

where Y is the dependent variable representing the adsorption capacity of DR-31; X_i and X_j are independent variables; β_0, β_i, β_{ii} and β_{ij} are migration coefficient, linear coefficient, second-order coefficient and interaction coefficient, respectively.

3. RESULTS AND DISSCUSSION

3.1. Characterization of Cu(PABA)

3.1.1. SEM and TEM analysis

SEM is a means of directly observing the morphology of materials, and the SEM image of Cu(PABA) is shown in Figure 1. As shown in Figure 1(a), Cu(PABA) presented as a spherical cluster as a whole, which is the same as the morphology reported by Yuan *et al.* (Yuan *et al.* 2021), but the surface thorn-like protrusions were obvious, which may be caused by different solvents. The thorn-like protrusions are more conducive to the increase of the surface area. In addition, there are many loose crystals that do not form spherical shapes next to the clusters, which may be due to the high rate of magnetic stirring during the synthesis process, which causes the crystals to be broken up after clustering, and their thorn-like characteristics are still obvious. Figure 1(b) shows the appearance of a single 'thorn' by transmission electron microscopy.

3.1.2. FT-IR analysis

The functional groups of Cu(PABA) were verified by FT-IR. The spectra are shown in Figure 2, and the peaks at 3,425 cm^{-1}, 3,253 cm^{-1} and 3,139 cm^{-1} can be attributed to the stretching of -OH,-NH and C-H (Jiang *et al.* 2022). The peaks at 1,610 cm^{-1} and 1,392 cm^{-1} may be caused by the vibration of carboxyl or benzene ring skeleton (Wang *et al.* 2019). The peak at 1,124 cm^{-1} is the in-plane bending vibration of C-H; the spectra at 825–638 cm^{-1} represent the out-of-plane bending vibration of C-H.

3.1.3. TGA analysis

Figure 3 shows the TGA results of Cu(PABA). The weight loss process can be divided into two stages. The first stage occurs between 30 °C and 230 °C, and the weight loss is about 7.5%, which is the loss process of non-coordinated water molecules and coordinated water molecules. 230–600 °C is the second stage of weight loss, the structure of Cu(PABA) is gradually destroyed and the skeleton collapses, and the mass loss is close to 70%. After 600 °C, there is no significant change in weight, which is a residue that exists stably in the form of CuO (Ramohlola *et al.* 2017). TGA shows that Cu(PABA) is stable when the temperature is lower than 230 °C.

Table 1 | Experimental design levels for the DR-31 dye adsorption factor on Cu(PABA)

			Levels		
Factors	**Unit**	**Code**	**−1**	**0**	**+1**
pH	–	A	10	11	12
Initial concentration	mg/L	B	150	200	250
Temperature	K	C	25°C	35°C	45°C

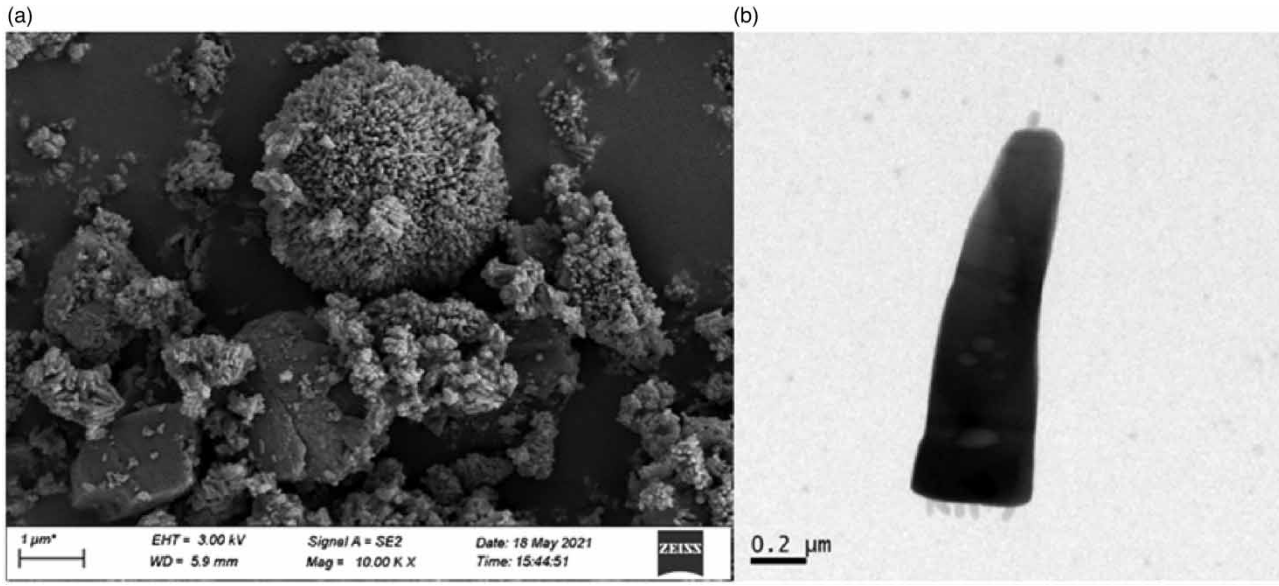

Figure 1 | The SEM (a) and TEM (b) images of Cu(PABA).

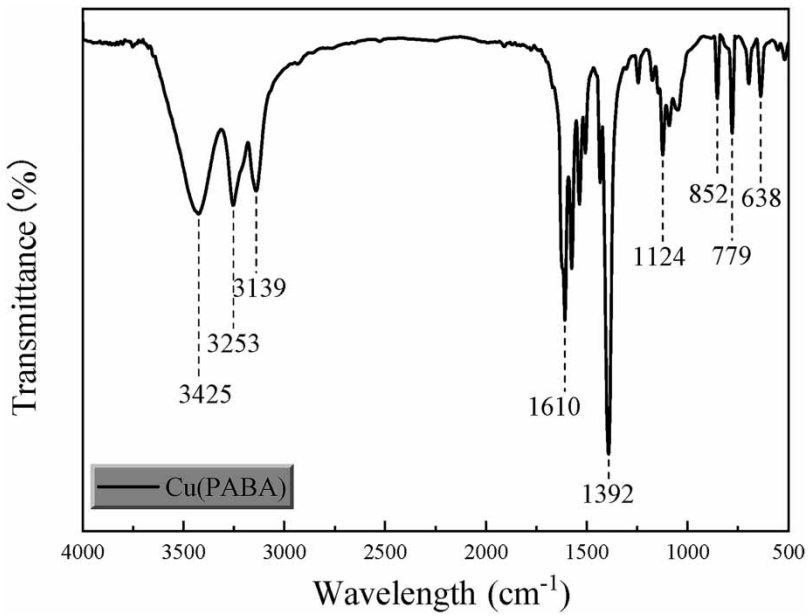

Figure 2 | FTIR spectrum of Cu(PABA).

3.1.4. BET analysis

The specific surface area and pore size distribution are important factors affecting the adsorption capacity of the adsorbent. Therefore, We used BET characterization to measure the specific surface area and pore size distribution of Cu(PABA). The N_2 adsorption-desorption isotherms of Cu(PABA) are shown in Figure 4. We can clearly see that the isotherm has an obvious hysteresis loop, which indicates that Cu(PABA) may have a mesoporous structure. The Characterization results show that the BET surface area of Cu(PABA) was obtained to 84 m^2/g. The Barrett-Joyner-Halenda (BJH) method was used to calculate the aperture, and the average aperture was obtained to 14.6 nm. The cumulative pore size adsorption and desorption volume were 0.076 m^3/g and 0.052 m^3/g, respectively. The inset in Figure 4. shows the pore distribution, and the pore size of Cu(PABA) mainly ranges from 1 to 40 nm.

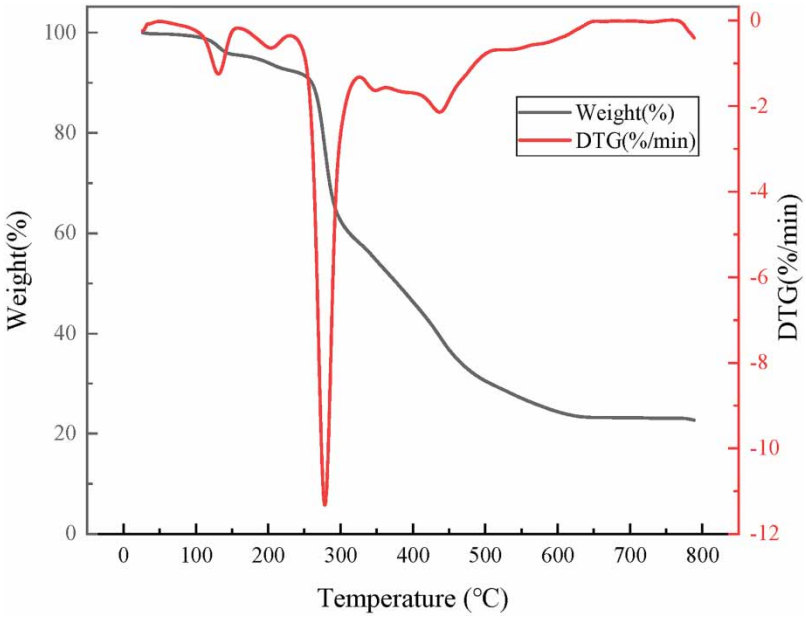

Figure 3 | TGA and DTG curve.

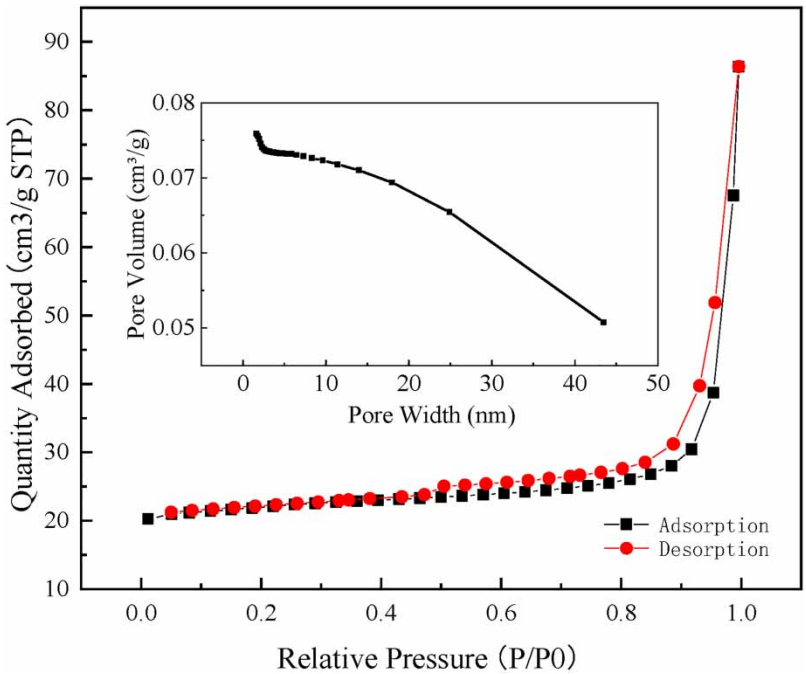

Figure 4 | N_2 adsorption–desorption curves and pore width distributions (inset) of Cu(PABA).

3.2. Effect of solution pH

pH is a non-negligible influencing factor, which can affect the surface charge of Cu(PABA) adsorbent and the ionization degree of DR-31 dye. We experimented the adsorption under the conditions of pH 3~12 at room temperature to analyze the effect of pH on the adsorption of DR-31 dye. Figure 5(a) shows the adsorption capacity of Cu(PABA) DR-31 under different pH conditions. We can see that the adsorption capacity is the lowest when pH=3. This may be attributed to the destruction of the structure of Cu(PABA) in a peracid environment. When the pH increased from 4 to 11, the adsorption capacity increased gradually with the

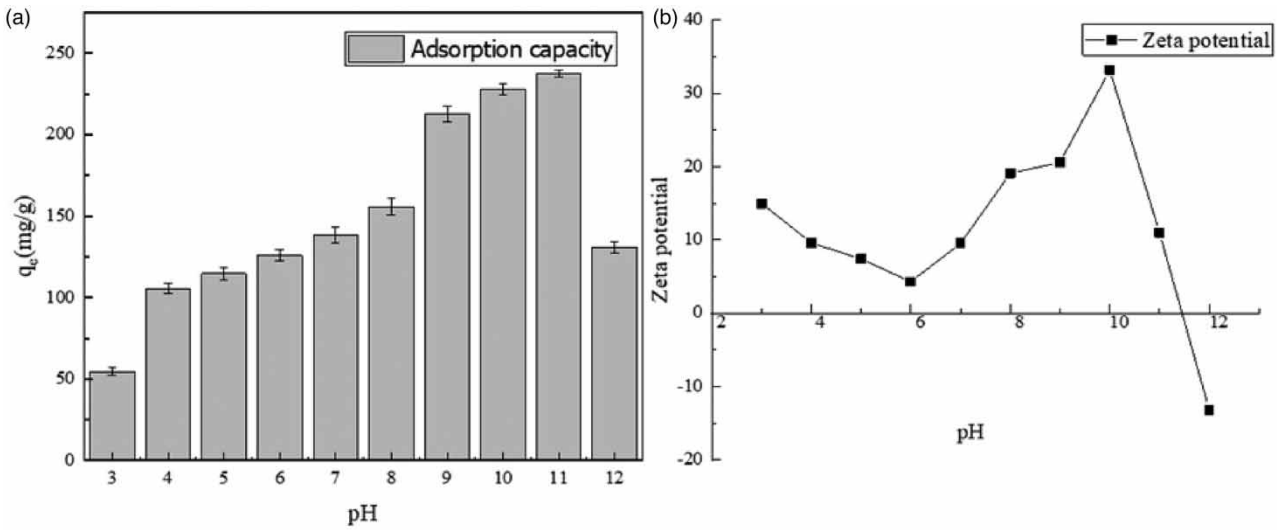

Figure 5 | (a) Effect of pH on the adsorption of Cu(PABA) toward DR-31; (b) The zeta potential of Cu(PABA) at various pHs.

increase of pH value. These trends can be explained by the Zeta potential of the material. As shown in Figure 5(b), the surface charge of Cu(PABA) maintains positive charge at pH lower than 11, and the Zeta potential approaches zero at pH=11, which is consistent with the experimental results of maximum adsorption capacity at pH=11. At this time, the adsorption capacity of Cu(PABA) for DR-31 was 237.7 mg/g, and the removal rate reached 95.6%. When pH>11, the adsorption capacity of Cu(PABA) began to decrease, which was due to the increase of the ionization degree of DR-31 at higher pH, the Zeta potential became negative charge and the electrostatic repulsion increased.

3.3. Effect of initial dye concentration

Figure 6(a) and 6(b) show the relationship between the initial concentration of DR-31 dye and the adsorption capacity and removal rate, respectively. The relationship between initial concentration and dye removal has been widely studied. Generally speaking, when the concentration is low, there are more adsorption sites and it is easier to adsorb. Thus there is a higher removal rate. As the initial concentration increases, it takes more time to reach equilibrium, while the adsorption sites are occupied and the adsorption rate decreases. Figure 6(b) shows that with the increase of the initial concentration of DR-31

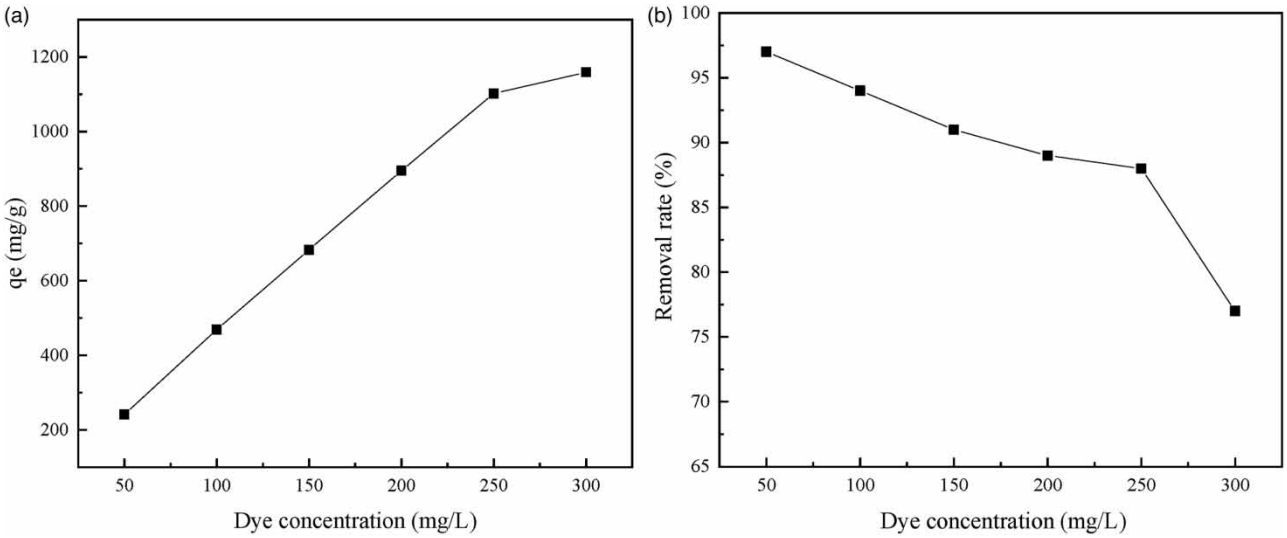

Figure 6 | (a) Effect of initial DR-31 concentration on Cu(PABA) adsorption capacity. (b) Variation of removal rate with increasing initial concentration.

dye, the removal rate shows a decreasing trend. During the process of increasing the initial concentration from 50 mg/L to 300 mg/L, the removal rate decreases from 95% to 77%, which can be attributed to the saturation of adsorbent adsorption sites. Figure 6(a) shows that with the increasing initial concentration, the adsorption capacity of the adsorbent at equilibrium also increases, which may be due to the increasing driving force due to the increasing concentration (Habibi *et al.* 2022).

3.4. Adsorption kinetics

Adsorption kinetics is an important experiment to explore the adsorption process, which can explain the adsorption mechanism and adsorption type. The kinetics were investigated using pseudo-first-order, pseudo-second-order and intraparticle diffusion models. They are described by Equations (4)–(6) respectively (Makrygianni *et al.* 2019; Saxena *et al.* 2020; Yang *et al.* 2021).

Pseudo-first-order kinetic model:

$$q_t = q_e(1 - e^{-kt}) \tag{4}$$

Pseudo-second-order kinetic model:

$$q_t = \frac{q_e v_0 t}{q_e + v_0 t} \tag{5}$$

Intraparticle diffusion equations:

$$q_t = k_p \cdot t^{1/2} + \mathrm{C} \tag{6}$$

In the above formula, q_t (mg/g) is the adsorption capacity at time t, and q_e (mg/g) represents the adsorption capacity at equilibrium; k (min^{-1}) and k_p (mg/g $\mathrm{min}^{0.5}$) represent pseudo-first-order rate constants and rate constants of internal diffusion, respectively; v_0 (mmol/(g·min) represents the initial adsorption rate for pseudo-second-order kinetics; C is a constant representing the thickness of the boundary layer in the intraparticle diffusion model.

Figure 7 and Table 2 show the simulation results and related parameter values of the kinetics, respectively. By comparing the values of the correlation coefficients in the table, it can be found that the R^2 (0.988) of the pseudo-first-order kinetic model is very close to the R^2 (0.980) of the pseudo-second-order kinetic model. Furthermore, the q_e (816.9 mg/g) calculated by the pseudo-first-order kinetic model is closer to the actual q_e value (744 mg/g). Therefore, it can be concluded that the pseudo-first-order model is more suitable to describe the adsorption of DR-31 by Cu(PABA).

In general, the adsorption process can include three steps: (1) the process of diffusion of the adsorbate from the bulk solution to the outer surface of the adsorbent, called out-diffusion; (2) The process in which the adsorbate enters the adsorbent micropores from the outer surface of the adsorbent and diffuses to the inner surface is called intraparticle diffusion; (3) The adsorbate is adsorbed by the adsorbent on the inner surface of the adsorbent solid, which is called the surface adsorption process. The intraparticle diffusion model was used to analyze the rate-limiting step of adsorption. If the graph shows a straight line through the origin, then the adsorption process is controlled only by intraparticle diffusion. If the graph does not show the origin or has multiple lines, it means that the adsorption process is not only controlled by intraparticle diffusion, but also affected by membrane diffusion and other diffusion mechanisms (Lin & Chang 2015; Zheng *et al.* 2021). It can be seen from Figure 7(c) that the adsorption process is divided into three stages and does not cross the origin, which indicates that the adsorption mechanism is affected by various diffusion mechanisms such as internal diffusion, membrane diffusion and surface adsorption.

3.5. Adsorption isotherms

In this study, two isotherm models of Langmuir (Xia *et al.* 2021) and Freundlich (Gao *et al.* 2018) were used for the analysis of the adsorption isotherm data.

Langmuir isotherm:

$$q_e = \frac{q_m b C_e}{1 + b C_e} \tag{7}$$

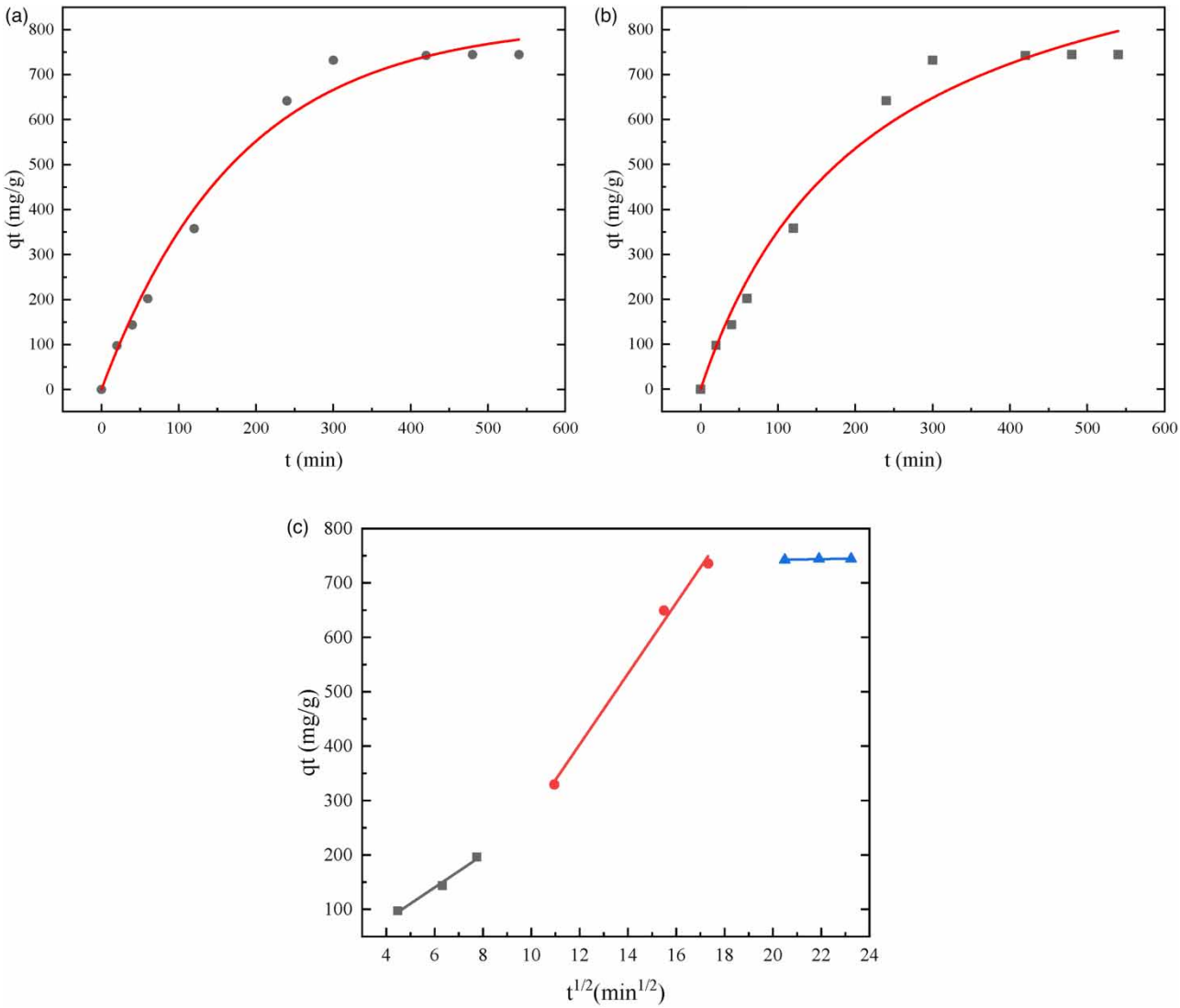

Figure 7 | The kinetic model of DR-31 dye adsorbed by Cu(PABA). (a) Pseudo-first-order; (b) Pseudo-second-order; (c) intraparticle diffusion.

Table 2 | Kinetic model parameters for the adsorption of DR-31 dye on Cu(PABA)

Model	Parameters	Value of parameters
Pseudo-first-order kinetic	k (min^{-1})	0.0056
	q_e (mg g^{-1})	816.9
	R^2	0.988
Pseudo-second-order kinetic	v_0 (mmol/(g min^{-1})	5.139
	q_e (mg g^{-1})	1,117.8
	R^2	0.980
Intraparticle diffusion	k_{p1} (mg g^{-1} $min^{-0.5}$)	29.881
	R^2	0.987
	k_{p2} (mg g^{-1} $min^{-0.5}$)	65.083
	R^2	0.994
	k_{p3} (mg g^{-1} $min^{-0.5}$)	0.695
	R^2	0.531

Freundlich isotherm:

$$q_e = KC_e^{\frac{1}{n}} \tag{8}$$

Above, C_e (mg/L) represents the equilibrium concentration of DR-31; q_e (mg/g) represents the adsorption capacity at equilibrium; q_m (mg/g) represents the maximum adsorption capacity; b (L/mg) and K ($mmol^{1-1/n}/g^{1-1/n}$) represent the Langmuir constant and Freundlich constant, respectively; n represents the heterogeneous factor related to the surface heterogeneity of adsorbent.

The Langmuir adsorption isotherm assumes that the adsorbent is a homogeneous surface, single molecular layer, and the adsorption site is limited, so the adsorption will reach saturation. The Freundlich model is an empirical model, assuming that the adsorption is on the heterogeneous solid surface, with multilayer adsorption. Figure 8(a) and 8(b) shows the Langmuir and Freundlich isotherms of Cu(PABA) at 298, 308 and 318 K, respectively. Table 3 lists the relevant parameters of each model and the parameters obtained at three temperatures. According to the correlation coefficient, the Langmuir model is more suitable for describing the adsorption of DR-31 dye on Cu(PABA). This indicates that the homogeneous monolayer adsorption assumed by the Langmuir model can better describe the adsorption of DR-31 dye on Cu(PABA).

Table 4 lists the maximum adsorption capacity of some reported dye adsorbents. It can be found that the maximum adsorption capacity of Cu(PABA) on DR-31 is significantly higher than that of many reported dye adsorbents. This indicates that Cu (PABA) is a promising adsorbent for DR-31 dye.

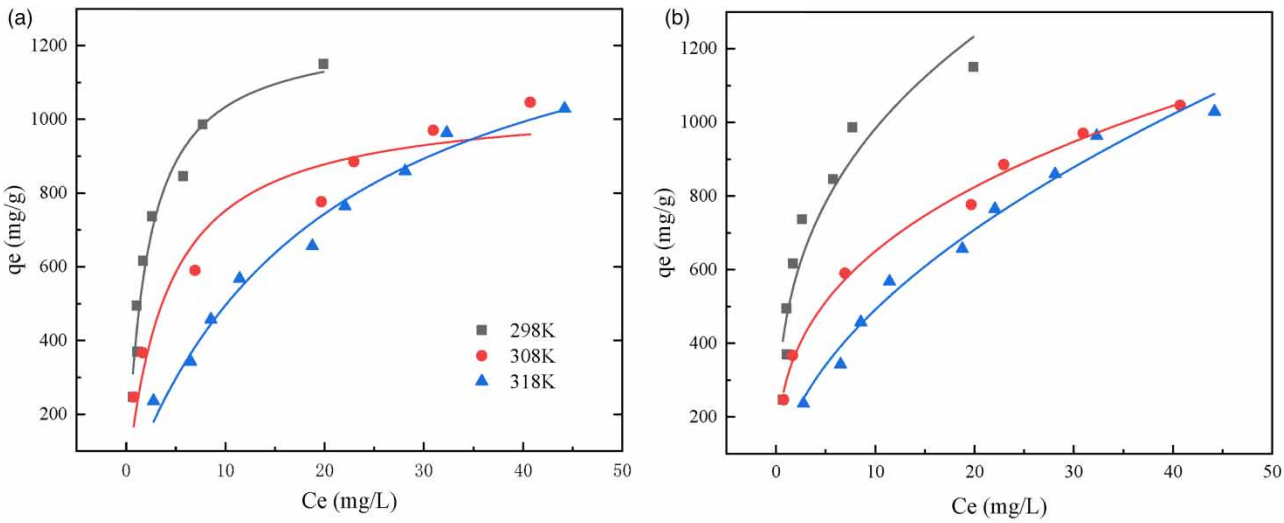

Figure 8 | Adsorption isotherms of DR-31 on Cu(PABA) at three temperatures (298 K, 308 K, 318 K): (a) Langmuir; (b) Freundlich.

Table 3 | Adsorption isotherm parameters for DR-31 adsorption on Cu(PABA)

		Value of parameters		
Isotherm	**Parameters**	**298 K**	**308 K**	**318 K**
Langmuir	q_m(mg g^{-1})	1,244.8	1,054.1	1,493.6
	b	0.490	0.249	0.050
	R^2	0.960	0.926	0.980
Freundlich	K	460.891	295.099	145.505
	n	3.041	2.917	1.892
	R^2	0.882	0.992	0.980

Table 4 | The reported adsorption capacity of DR-31 dye adsorbent

Adsorbents	Tempenture(°C)	Adsorption capacity (mg/g)	References
Cu(PABA)	25	1,244.8	This study
Biochar-Cp	25	136.7	Behl *et al.* (2019)
Rice husk	30	129.8	Safa & Bhatti (2011)
$NiFe_2O_4$/AC	25	299.7	Livani & Ghorbani (2018)
Activated carbon	25	111.0	Mahmoodi *et al.* (2011)
Surfactant-modified coconut coir pith	32	76.3	Sureshkumar & Namasivayam (2008)
Core–shell magnetic adsorbent nanoparticle	25	323	Mahmoodi (2014)
Garlic peel	55	38.0	Asfaram *et al.* (2014)
Fe (III)/Cr (III) hydroxide	25	5.1	Namasivayam & Sumithra (2005)

3.6. Adsorption mechanism

DR-31 is a direct dye soluble in water in an anionic state. We measured the zeta potential of Cu(PABA), which is greater than zero at pH values less than 11, electrostatically attracting the negatively charged DR-31 dye. Electrostatic interaction is one of the main mechanisms affecting the adsorption of dyes on MOFs (Li *et al.* 2018). BET characterization showed that Cu(PABA) has mesopores with an average pore size as high as 14.6 nm, which facilitates the entry of DR-31 molecules into the pores of Cu(PABA) and is an important factor leading to the high adsorption capacity. To further explore the mechanism of adsorption, we performed XSP scans of Cu(PABA) before and after adsorption. Broad-scan XPS spectra showed peaks of C1 s, N1 s, O1 s and Cu2p, which are the main constituent elements of Cu(PABA). As shown in Figure 9(c), a new peak appeared at 400.6 eV in the high-resolution spectrum of N1 s after adsorption. This could be NH3+, which illustrates the protonation process of the amino group, making the material positively charged at low pH, which favors electrostatic attraction (Valadi *et al.* 2022). A new peak appeared in the high-resolution spectrum of S2p, which was related to -SO_3 of the direct dye, indicating that DR-31 was successfully adsorbed onto Cu(PABA). In addition, hydrogen bonding and π-π interactions have also been reported to be important mechanisms affecting the adsorption of dye molecules (Tchinsa *et al.* 2021).

3.7. RSM analysis

The ANOVA results for DR-31 dye adsorption by Cu(PABA) are shown in Table 5. Through Design Expert program, the experimental results were fitted to the following equation.

$$Y(\%) = 97.56 - 9.09A - 1.01\mathrm{B} - 4.28\mathrm{C} - 0.375\mathrm{AB} + 0.5\mathrm{AC} - 1.55\mathrm{BC} - 71.64\mathrm{A}^2 - 0.6925\mathrm{B}^2 - 2.97\mathrm{C}^2 \quad (9)$$

where Y is defined as the removal rate of DR-31, A is pH, B is the initial concentration of DR-31dye (mg/g), and C is temperature (°C). In the variance analysis, the significance of model was determined using the *P*-values and F-values and the higher the value of F and the lower value of P, the more the significance of the model would be (Nguyen *et al.* 2022). Here, F value=137.8, p (<0.0001), indicating that the model is significant and can well explain the removal of DR-31. As can be seen in Table 5, there are A, B, A^2 and C^2 with p-value <0.05, which shows that these terms are important model terms. In addition, the value of the determination coefficient R^2 is 0.9980, the adjusted R^2 value is equal to 0.9954, and the predicted R^2 value is equal to 0.9877. High R^2 values indicate the reliability of the OR model in predicting response. High R^2 values indicate the reliability of the OR model in predicting response. Figure 10(a)–10(c) shows the interaction of pH-initial concentration, pH-temperature and initial concentration-temperature in the selected variable range. It can be found that there is a weak interaction between the independent variable and its optimal response.

Based on the fitted model,the optimal DR-31 adsorption conditions are: pH=10.9, Initial concentration=216.6 mg/g, Temperature=27 °C, and removal efficiency reached 99.4%. In order to verify the prediction results, we conducted experimental tests, and the results showed that the direct deviation between the prediction results and the experimental results was very small (<3%), which verified the validity of the model.

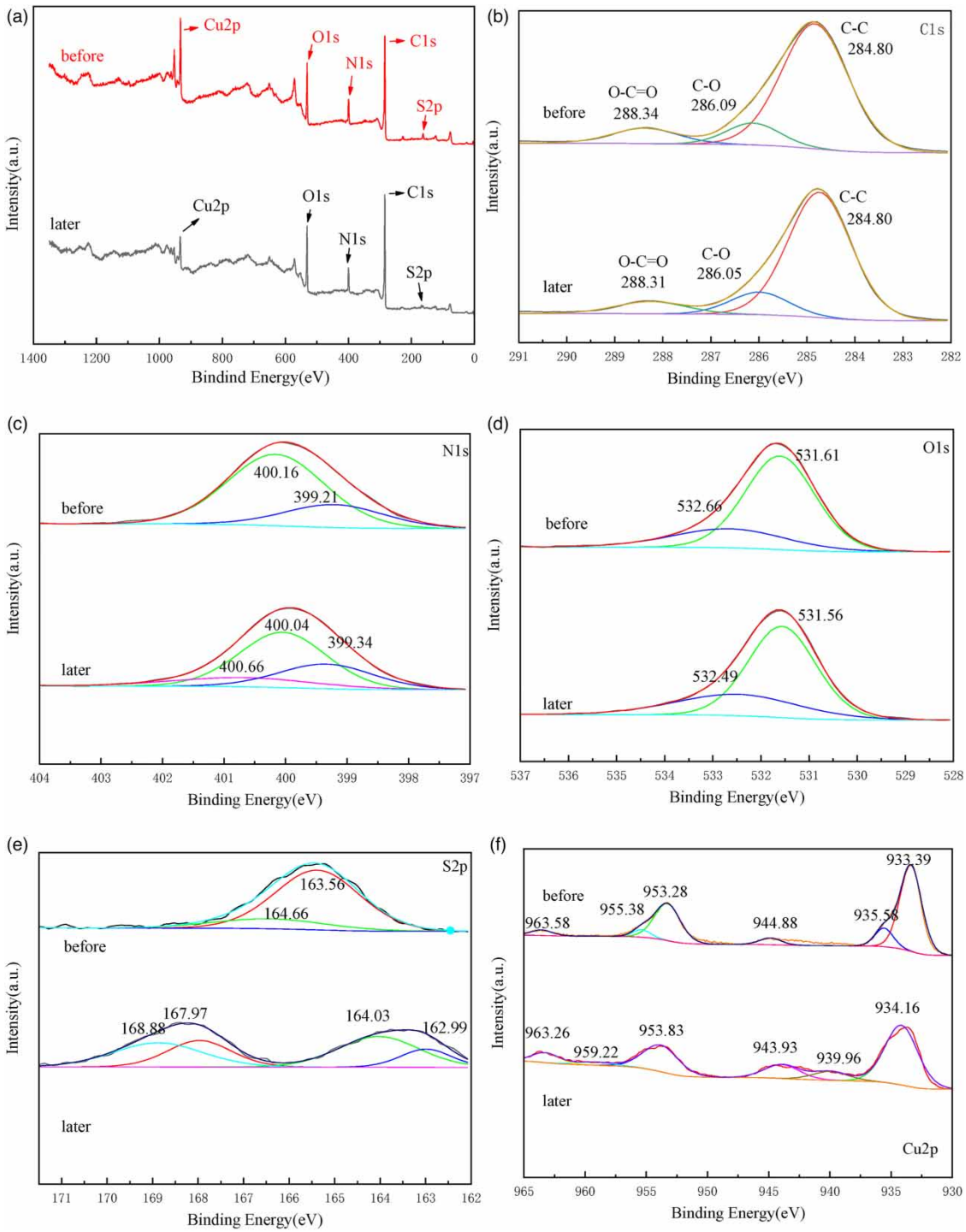

Figure 9 | XPS spectra of Cu(PABA) before and after adsorption of DR-31. (a) full view; (b) C1 s; (c) N 1 s; (d) O1 s; (e) S2p; (f) Cu2p.

4. CONCLUSOINS

In this study, Cu(PABA) was synthesized by a solvothermal method and used to remove DR-31 dye from aqueous solution. The characterization results show that Cu(PABA) has mesoporous structure with high surface area (84 m^2/g) and large average pore size (14.6 nm). Therefore, Cu(PABA) has strong adsorption capacity and can effectively remove DR-31 dye in water.

Table 5 | ANOVA data for the DR-31 adsorption model

Source	Sum of squares	df	Mean square	F-value	*p*-value	
Model	22,728.20	9	2,525.36	383.05	<0.0001	significant
A	660.66	1	660.66	100.21	<0.0001	
B	8.20	1	8.20	1.24	0.3015	
C	146.21	1	146.21	22.18	0.0022	
AB	0.5625	1	0.5625	0.0853	0.7787	
AC	1.0000	1	1.0000	0.1517	0.7085	
BC	9.61	1	9.61	1.46	0.2665	
A^2	21,611.15	1	21,611.15	3,278.00	<0.0001	
B^2	2.02	1	2.02	0.3063	0.5972	
C^2	37.08	1	37.08	5.62	0.0495	
Residual	46.15	7	6.59			
Lack of fit	14.42	3	4.81	0.6058	0.6453	not significant
Pure error	31.73	4	7.93			
Cor total	22,774.35	16				

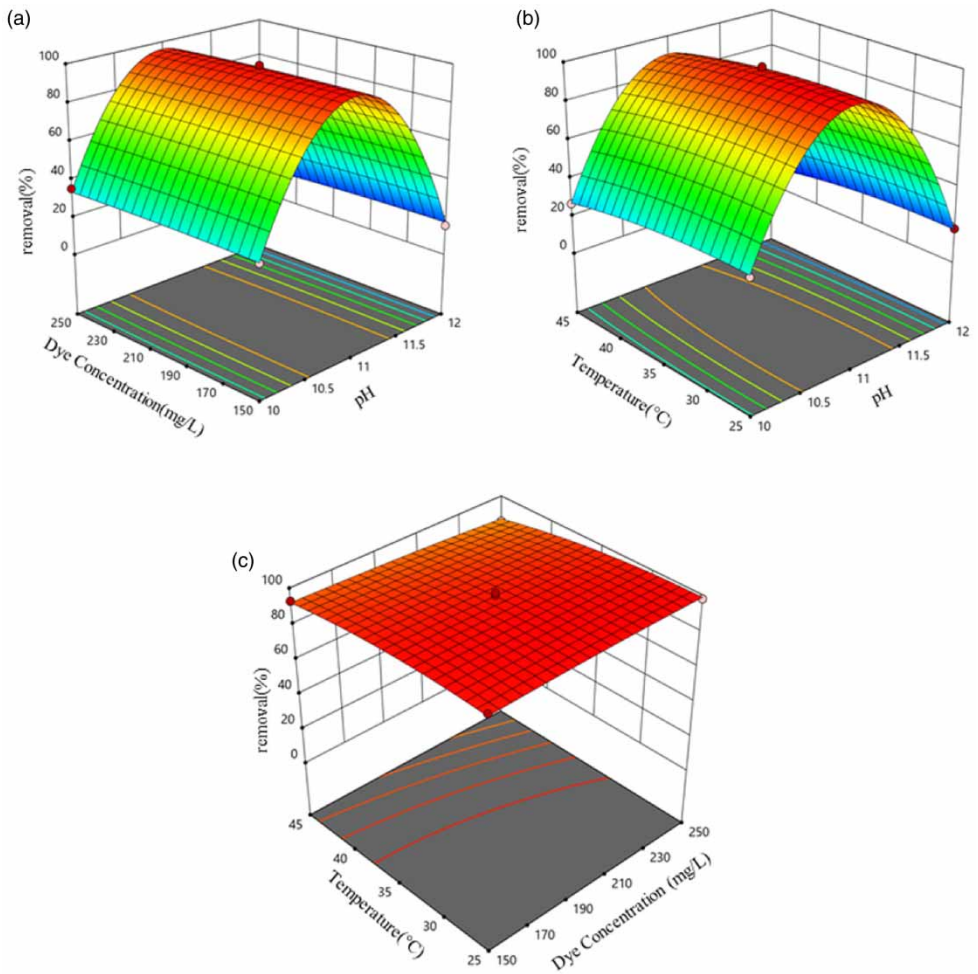

Figure 10 | The 3D response surface plot for the interaction of the pH, initial DR-31 dye concentration and temperature.

According to the langmuir model, the maximum adsorption capacity reached 1,244.8 mg/g. Adsorption experiments showed that the adsorption of Cu(PABA) on DR-31 dye was more in line with langmuir isotherm model and quasi-first-order kinetic model. Based on the optimization results of response surface, the removal rate was 99.4% under the optimal conditions of pH(10.9), DR-31 dye concentration (216.6 mg/L) and temperature (27 °C). In summary, Cu(PABA) was a promising adsorbent for dyes. Further study on the adsorption mechanism and more experiments on different dyes are necessary.

ACKNOWLEDGEMENTS

This work was supported by Science and Technology Innovation Team Project of Hubei Provincial Department of Education (Grant No. T2020002), Wuhan Science and Technology Planning Project (Grant No. 2020020601012274), National Natural Science Foundation of China (Grant No. 41571306) and Hubei Technological Innovation Special Fund (Grant No. 2020ZYYD019). The authors would like to thank Jiang Lang from Shiyanjia Lab (www.shiyanjia.com) for the characterization support.

DATA AVAILABILITY STATEMENT

All relevant data are included in the paper or its Supplementary Information.

CONFLICT OF INTEREST STATEMENT

The authors declare there is no conflict.

REFERENCES

Asfaram, A., Fathi, M. R., Khodadoust, S. & Naraki, M. 2014 Removal of direct Red 12B by garlic peel as a cheap adsorbent: kinetics, thermodynamic and equilibrium isotherms study of removal. *Spectrochimica Acta Part A: Molecular and Biomolecular Spectroscopy* **127**, 415–421.

Behl, K., Sinha, S., Sharma, M., Singh, R., Joshi, M., Bhatnagar, A. & Nigam, S. 2019 One-time cultivation of Chlorella pyrenoidosa in aqueous dye solution supplemented with biochar for microalgal growth, dye decolorization and lipid production. *Chemical Engineering Journal* **364**, 552–561.

Bhatia, S., Verma, N. & Bedi, R. K. 2016 Optical application of Er-doped ZnO nanoparticles for photodegradation of direct red - 31 dye. *Optical Materials* **62**, 392–398.

Chowdhury, M. F., Khandaker, S., Sarker, F., Islam, A., Rahman, M. T. & Awual, M. R. 2020 Current treatment technologies and mechanisms for removal of indigo carmine dyes from wastewater: a review. *Journal of Molecular Liquids* **318**, 114061.

Faisal, A. A. H., Ramadhan, Z. K., Al-Ansari, N., Sharma, G., Naushad, M. & Bathula, C. 2022 Precipitation of (Mg/Fe-CTAB) - Layered double hydroxide nanoparticles onto sewage sludge for producing novel sorbent to remove Congo red and methylene blue dyes from aqueous environment. *Chemosphere* **291**, 132693.

Gao, Y., Liu, K., Kang, R., Xia, J., Yu, G. & Deng, S. 2018 A comparative study of rigid and flexible MOFs for the adsorption of pharmaceuticals: kinetics, isotherms and mechanisms. *Journal of Hazardous Materials* **359**, 248–257.

Habibi, M. K., Rafiaei, S. M., Alhaji, A. & Zare, M. 2022 Synthesis of ZnFe2O4: 1 wt% Ce3 + /Carbon fibers composite and investigation of its adsorption characteristic to remove Congo red dye from aqueous solutions. *Journal of Alloys and Compounds* **890**, 161901.

Jiang, S., Ren, D., Wang, Z., Zhang, S., Zhang, X. & Chen, W. 2022 Improved stability and promoted activity of laccase by one-Pot encapsulation with Cu (PABA) nanoarchitectonics and its application for removal of Azo dyes. *Ecotoxicology and Environmental Safety* **234**, 113366.

Katheresan, V., Kansedo, J. & Lau, S. Y. 2018 Efficiency of various recent wastewater dye removal methods: a review. *Journal of Environmental Chemical Engineering* **6** (4), 4676–4697.

Li, T., Liu, Y., Wang, T., Wu, Y., He, Y., Yang, R. & Zheng, S. 2018 Regulation of the surface area and surface charge property of MOFs by multivariate strategy: synthesis, characterization, selective dye adsorption and separation. *Microporous and Mesoporous Materials* **272**, 101–108.

Lin, K. Y. & Chang, H. A. 2015 Ultra-high adsorption capacity of zeolitic imidazole framework-67 (ZIF-67) for removal of malachite green from water. *Chemosphere* **139**, 624–631.

Livani, M. J. & Ghorbani, M. 2018 Fabrication of nife2o4 magnetic nanoparticles loaded on activated carbon as novel nanoadsorbent for Direct Red 31 and Direct Blue 78 adsorption. *Environmental Technology* **39** (23), 2977–2993.

Mahmoodi, N. M. 2014 Synthesis of core–shell magnetic adsorbent nanoparticle and selectivity analysis for binary system dye removal. *Journal of Industrial and Engineering Chemistry* **20** (4), 2050–2058.

Mahmoodi, N. M., Salehi, R. & Arami, M. 2011 Binary system dye removal from colored textile wastewater using activated carbon: kinetic and isotherm studies. *Desalination* **272** (1–3), 187–195.

Makrygianni, M., Lada, Z. G., Manousou, A., Aggelopoulos, C. A. & Deimede, V. 2019 Removal of anionic dyes from aqueous solution by novel pyrrolidinium-based Polymeric Ionic Liquid (PIL) as adsorbent: investigation of the adsorption kinetics, equilibrium isotherms and the adsorption mechanisms involved. *Journal of Environmental Chemical Engineering* **7** (3), 103163.

Namasivayam, C. & Sumithra, S. 2005 Removal of direct red 12B and methylene blue from water by adsorption onto Fe (III)/Cr (III) hydroxide, an industrial solid waste. *Journal of Environmental Management* **74** (3), 207–215.

Nguyen, V., Vo, T., Nguyen, T., Dat, N. D., Huu, B. T., Nguyen, X., Tran, T., Le, T., Duong, T., Bui, M., Dong, C. & Bui, X. 2022 Adsorption of norfloxacin from aqueous solution on biochar derived from spent coffee ground: master variables and response surface method optimized adsorption process. *Chemosphere (Oxford)* **288** (2), 132577.

Oladoye, P. O., Adegboyega, S. A. & Giwa, A. A. 2021 Remediation potentials of composite metal-organic frameworks (MOFs) for dyes as water contaminants: a comprehensive review of recent literatures. *Environmental Nanotechnology, Monitoring & Management* **16**, 100568.

Ramohlola, K. E., Masikini, M., Mdluli, S. B., Monama, G. R., Hato, M. J., Molapo, K. M., Iwuoha, E. I. & Modibane, K. D. 2017 Electrocatalytic hydrogen evolution reaction of metal organic frameworks decorated with poly (3-aminobenzoic acid). *Electrochimica Acta* **246**, 1174–1182.

Sadiq, A. C., Olasupo, A., Ngah, W. S. W., Rahim, N. Y. & Suah, F. B. M. 2021 A decade development in the application of chitosan-based materials for dye adsorption: a short review. *International Journal of Biological Macromolecules* **191**, 1151–1163.

Safa, Y. & Bhatti, H. N. 2011 Kinetic and thermodynamic modeling for the removal of Direct Red-31 and Direct Orange-26 dyes from aqueous solutions by rice husk. *Desalination* **272** (1–3), 313–322.

Saxena, M., Sharma, N. & Saxena, R. 2020 Highly efficient and rapid removal of a toxic dye: adsorption kinetics, isotherm, and mechanism studies on functionalized multiwalled carbon nanotubes. *Surfaces and Interfaces* **21**, 100639.

Sureshkumar, M. V. & Namasivayam, C. 2008 Adsorption behavior of Direct Red 12B and Rhodamine B from water onto surfactant-modified coconut coir pith. *Colloids and Surfaces A: Physicochemical and Engineering Aspects* **317** (1–3), 277–283.

Tchinsa, A., Hossain, M. F., Wang, T. & Zhou, Y. 2021 Removal of organic pollutants from aqueous solution using metal organic frameworks (MOFs)-based adsorbents: a review. *Chemosphere* **284**, 131393.

Valadi, F. M., Shahsavari, S., Akbarzadeh, E. & Gholami, M. R. 2022 Preparation of new MOF-808/chitosan composite for Cr(VI) adsorption from aqueous solution: experimental and DFT study. *Carbohydrate Polymers* **288**, 119383.

Wang, L., Zhi, W., Wan, J., Han, J., Li, C. & Wang, Y. 2019 Recyclable β-Glucosidase by one-pot encapsulation with Cu-MOFs for enhanced hydrolysis of cellulose to glucose. *ACS Sustainable Chemistry & Engineering* **7** (3), 3339–3348.

Xia, J., Gao, Y. & Yu, G. 2021 Tetracycline removal from aqueous solution using zirconium-based metal-organic frameworks (Zr-MOFs) with different pore size and topology: adsorption isotherm, kinetic and mechanism studies. *Journal of Colloid and Interface Science* **590**, 495–505.

Yang, X., Zhu, W., Song, Y., Zhuang, H. & Tang, H. 2021 Removal of cationic dye BR46 by biochar prepared from chrysanthemum morifolium Ramat straw: a study on adsorption equilibrium, kinetics and isotherm. *Journal of Molecular Liquids* **340**, 116617.

Yuan, Y., Cai, W., Xu, J., Cheng, J. & Du, K. 2021 Recyclable laccase by coprecipitation with aciduric Cu-based MOFs for bisphenol A degradation in an aqueous environment. *Colloids and Surfaces B: Biointerfaces* **204**, 111792.

Zheng, X., Qiu, C., Long, J., Jiao, A., Xu, X., Jin, Z. & Wang, J. 2021 Preparation and characterization of porous starch/β-cyclodextrin microsphere for loading curcumin: equilibrium, kinetics and mechanism of adsorption. *Food Bioscience* **41**, 101081.

First received 21 March 2022; accepted in revised form 7 June 2022. Available online 13 June 2022